Effect of Temperature on Structure and Electronic Properties of Nanometric Spinel-Type Cobalt Oxides

G. Godillot, L. Guerlou-Demourgues,* L. Croguennec, K. M. Shaju, and C. Delmas

CNRS, Université de Bordeaux, ICMCB, 87 Avenue du Dr. A. Schweitzer, Pessac, F 33608, France

ABSTRACT: Temperature is shown to have a huge influence on the electronic properties of nanometric spinel type cobalt oxides precipitated at low temperature in alkaline media. The initial phase, with formula $H_xLi_yCo_{3-\delta}O_4$, contains hydrogen, lithium, cobalt vacancies, and a mixed valence Co^{4+}/Co^{3+} within the structure, leading to an electronic conductivity higher than that of stoichiometric Co_3O_4. Its structural evolution under thermal treatment was studied by X ray diffraction and chemical analysis, which reveal modifications in structure and compositions, involving water release, increase of the Co/O atomic ratio, and modification of the Co^{4+}/Co^{3+} ratio. The RT to 300 °C range is particularly interesting as a single phase domain and the materials obtained in this temperature range were investigated by chemical analysis, electronic conductivity and specific surface area measurements. Upon increasing temperature, the enhancement of the Co^{4+}/Co^{3+} ratio, together with cationic redistribution in the spinel framework, results in an improvement of the electronic conductivity (more than 2 orders of magnitude for materials heated above 150 °C). Finally, the systematic thermal study of electronic conductivity and specific surface area of the materials allows to determine an optimal heat treatment temperature leading to an optimized active electrode material for electrochemical energy storage applications, especially in supercapacitors. Such a solid state chemistry approach combining many material characterization techniques to reach a complete knowledge of the material is quite rare in the literature concerning oxides for supercapacitors.

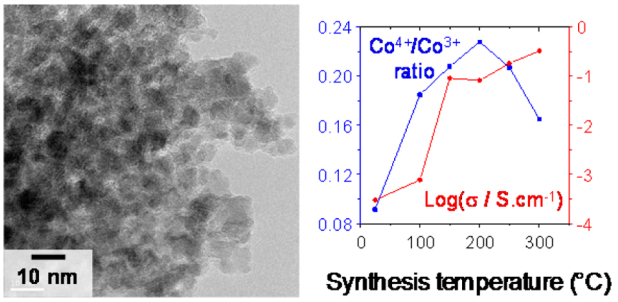

INTRODUCTION

Co_3O_4 has been extensively studied in a wide range of applications such as catalysis (mainly for the treatment of waste gases),[1−3] sensing,[4,5] or magnetism.[6,7] It is also particularly considered in electrochemical energy storage, as negative electrode material in lithium batteries[8,9] or in supercapaci tors.[10,11] In this last field, increasing capacities, which are highly dependent on specific surface area and pore size distribu tion,[10,12] requires to prepare very small particles. One way to achieve this goal is the "chimie douce" approach, low energy consuming, and which enables to prepare nanometric powders with controlled texture and morphology. It is also known to promote the precipitation of kinetically metastable phases, including materials with many defects that can exhibit original and interesting properties.

Co_3O_4 crystallizes in a normal spinel structure (space group *Fd*3*m*), which can be described as a three dimensional $[Co_2O_4]$ framework of Co^{3+} ions in edge sharing octahedral sites (16d), with empty channels in the three space directions. Co^{2+} ions are located in tetrahedral sites (8a), at the intersection of the channels, and share only corners with the octahedra. The electronic transfer between Co^{2+} ions in tetrahedral sites and Co^{3+} ions in octahedral sites is impossible since Co^{3+} ions are not stabilized in tetrahedral environment, and occurs only between Co^{3+} ions (t_{2g}^6 LS) across the shared edges of the CoO_6 octahedra. Therefore, Co_3O_4 is a semiconductor with a poor electronic conductivity.[13]

The spinel structure is well known to accommodate a wide range of metal cations with different oxidation states. Substituted cobaltites were already explored by Holgersson et al.[14] More recently, Pyke et al. studied the substitution of many transition elements (Li, Cu, Al, Ga, Mn, Ti, Sn, Ge) for cobalt in Co_3O_4 and concluded to the existence of solid solutions in all cases.[15] Ni doped[16] and K doped[17] Co_3O_4 were also inves tigated, but most of works focus on Li doping, showing a significant improvement in electronic conductivity.[8,13,18−20] This property was mainly explained by the presence of Co^{4+} to ensure charge balance when lithium is substituted for Co^{2+} or Co^{3+}, thus, allowing delocalization of holes in the octahedral network, and leading therefore to conductivities higher than that of stoichiometric Co_3O_4. Depending on synthesis conditions (precursors, temperature), Li ions were determined to occupy 8a sites,[18] 16d sites,[13] and interstices,[8] but were also identified to be distributed in several spinel sites.[19,21] In particular, micrometric spinel type cobalt oxides containing H and Li in the structure were prepared in our group by electrochemical oxidation of CoO.[22] Such materials were

shown to contain hydrogen and lithium ions, as well as cobalt vacancies in both tetrahedral and octahedral sites. It was demonstrated that cobalt vacancies are compensated by H^+ and Li^+ ions, but also by the presence of Co^{4+} ions. As a result, very good electronic properties could be achieved, with electronic conductivity higher by 4 or 5 decades (at room temperature), as compared with stoichiometric Co_3O_4.[22] It has also been highlighted that a moderate thermal treatment leads to an additional increase of conductivity, due to modifications in structure/composition, involving water release and increase of the Co/O atomic ratio.[23,24]

More recently, materials with similar composition but nanometric size were prepared.[25] These materials, denoted as nano Co_3O_4 in the following, are synthesized by precipitation at low temperature in various alkaline media. They also show high electronic conductivity, as well as the presence of lithium, hydrogen, and cobalt vacancies. According to the first results we recently reported, these nano Co_3O_4 phases are promising candidates as electrodes materials for hybrid supercapacitors,[26] thanks to a high conductivity and a high specific surface induced by their nanometric size. The present paper will study on the effect of temperature, focusing on the relationships between structure, chemical composition, and electronic properties.

EXPERIMENTAL SECTION

Material Preparation. As described in detail in a previous paper,[25] the initial nano Co_3O_4 type phase was prepared by precipitation at 90 °C of a cobalt salt in a 8 M KOH + 0.5 M NaOH + 0.5 M LiOH alkaline solution. Cobalt nitrate hexahydrate (Fluka) was thus dissolved into distilled water, mixed with hydrogen peroxide (Fluka; with a $Co(NO_3)_2/H_2O_2$ molar ratio of 3:2), and then added dropwise to the ternary alkaline solution to induce precipitation of the nanometric cobalt oxide. The suspension obtained was allowed to ripen for 4 h at 90 °C. Afterward, the precipitate was centrifugated and washed with distilled water until neutrality and then dried at 60 °C for 24 h. The resulting powder was finally ground in a pestle and mortar. As nanometric materials, all the synthesized samples tend to adsorb large amounts of molecules contained in air (especially water) and were, therefore, stored in a desiccator to keep a constant and low amount of adsorbed water. Reference high temperature Co_3O_4 (HT Co_3O_4) was obtained from the thermal treatment of cobalt carbonate (Alfa Aesar), at 450 °C, under an oxygen flow for 15 h.

Heat Treatment. The initial nano Co_3O_4 powder was subjected to heat treatments, under air, at temperatures ranging from 100 to 650 °C (100, 150, 200, 250, 300, 400, and 650 °C). These temperatures were determined on the basis of the X ray diffraction in situ analysis, taking into account that thermal analysis shows a continuous loss of water from room temperature and a decomposition of Co_3O_4 into CoO after 650 °C, as evidenced elsewhere.[27] The temperature was increased at the rate of 2 °C/min up to the target temperature, held for a 4 h isothermal stage and then decreased down to room temperature at 2 °C/min. All the heat treatments were performed ex situ on the same starting material to investigate accurately the effect of temperature on the parameters studied, especially on the chemical composition. The starting fresh precipitated material is denoted as SP initial ("SP" for spinel), while the heated samples are called SP 100, SP 150, ..., SP 650, depending on the treatment temperature.

Characterization. Both in situ and ex situ analysis were carried out on nano Co_3O_4. In situ analysis consisted of studying the evolution of the X ray diffraction pattern of SP initial sample with temperature. For ex situ analysis, SP initial and the seven heat treated samples (SP initial to SP 650) were investigated, at room temperature, by means of X ray diffraction, chemical analysis, specific surface area and electronic conductivity measurements.

To carry out in situ analysis, heat treatment was coupled with X ray diffraction analysis by connecting an Anton Paar HTK 1200 high temperature furnace to the diffractometer. The sample was placed in a variable temperature chamber under air, and a first acquisition was performed at room temperature. Then, the temperature of the chamber was gradually increased up to 650 °C (3 °C/min), and X ray data acquisition was performed during the 4 h isothermal stages (every 50 °C). Then, a symmetrical process was applied during the cooling down of the chamber, and a last X ray diagram was recorded at room temperature.

In thermal in situ analysis, X ray diffraction (XRD) data were collected with a Philips PANalytical X'Pert Pro diffractometer using the cobalt Kα radiation. The powder diffraction patterns were recorded for around 4 h (2.41 s per step) in the 10−110° (2θ) angular range, with a 0.0167° (2θ) step size and a 2.122° (2θ) active width in the detector. Similar conditions were used to record ex situ XRD patterns but with longer acquisition time (11 h, 6.44 s per step).

Structure refinements were based on the Rietveld[28] method using the FullProf program.[29] The diffraction peaks were fitted with a pseudo Voigt function $PV = \eta L + (1 - \eta)G$, η being the Lorentzian contribution to the Gaussian peak shape. Lattice parameters, parameters of the profile function (η, U, V, W), position of oxygen, cobalt occupancies, and isotropic atomic displacement parameters (B) were refined. Moreover, the materials studied are poorly crystallized and exhibit a strong and angular dependent background. A polynomial function with six refined parameters was therefore chosen to describe it. Finally, using the Scherrer's formula, the instrumental width was neglected, compared to the broad peaks exhibited by the nanometric materials studied.

Specific surface area measurements were carried out on a Quantachrome Instruments Autosorb 1. For each sample, around 30 mg of material was degassed at 150 °C for 15 h under helium, and an adsorption/desorption isotherm was recorded under nitrogen for relative pressures ranging from 0.02 to 0.99. All the isotherms obtained revealed to be type IV isotherms,[30] that is, characteristics of a mesoporous material. Consequently, for every material, specific surface area could be determined using the BET theory[31,32] on adsorption isotherm for $P/P^0 < 0.35$ (identical results were obtained from desorption isotherms).

Chemical analysis was performed by Inductive Coupled Plasma (on a Varian 720 ES ICP OES) for Li, Na, K, and Co titration, and by elementary microanalysis (on a Thermo flash EA 1112 Series CHNS analyzer) for H and C titration. The average oxidation state of cobalt was established by the iodometric titration method. Cobalt ions at an oxidation state higher than 2 in the material can be reduced to Co^{2+} by I^- ions (from KI solution), I^- being oxidized into I_2. Back titration of previously formed I_2 by $S_2O_3^{2-}$ (0.1 M $Na_2S_2O_3$) allows the average oxidation state of cobalt to be deduced. Around 30 mg of material was introduced in a PTFE container with 5 mL of H_2O, 10 mL of 10 g/L KI, and 5 mL of 12 M HCl. A second

container, constituting a reference sample, was prepared with the same solutions but no powder. Both containers were sealed and heated in an oven at 60 °C for 20 h to complete dissolution and reduction of the material. Such a method is particularly useful to dissolve cobalt oxide powders while avoiding evaporation of I_2 at high temperatures. However, it must be noticed that Cl^- ions from the hydrochloric acid solution (which is used for the dissolution of the material) can also reduce Co^{n+} ions ($n > 2$). The 5 mL of HCl were consequently added carefully at the very end of the container filling, to avoid direct contact with the material. Back titration was finally performed after the cooling of the containers. The titrated volume of the reference sample was subtracted in order to consider the oxidizing effect of dissolved oxygen. With the aim of following the evolution of cobalt average oxidation state upon temperature, efforts have been made to minimize as much as possible the uncertainty on the measurement by carrying out a large number of analyses; especially to limit the influence of the titrated volume of the reference sample which was found to vary among experiments.

Temperature dependent electronic conductivity measurements were carried out on 8 mm diameter pellets with the four probe technique,[33] using a direct current. Each value of electronic conductivity is determined from the measurement of the potential resulting from the application of a DC current in both positive and negative sense (according to the four probe technique) in order to avoid stray voltages and therefore to get rid of the diode effect. The temperature was progressively raised to 400 °C and then cooled down to room temperature at a rate of 1 °C/min. The pellets were obtained by compacting around 200 mg of powder at 8 t/cm^2 (thickness close to 1.2 mm and density close to 3.3 g/cm^3). Because of the low temperature synthesis of the materials, the pellets could not be sintered.

RESULTS AND DISCUSSION

1. Structure and Morphology. *Starting Material.* The X ray diffraction diagram of the fresh precipitated material (SP initial) is compared in Figure 1 with that of a reference HT Co_3O_4 phase. It shows the presence of a pure phase, with spinel structure, isotypic with the HT Co_3O_4 one. The pattern of SP initial exhibits very broad diffraction peaks, which confirm the presence of nanometric coherent domains. By applying the Scherrer's formula on the most intense four peaks ((220), (311), (511), and (440)), their size has been estimated to stay close to 5 nm, in agreement with that determined by TEM measurements.[26] In addition, an inversion of the (220)/(111) line intensity ratio can be noticed in Figure 1 between SP initial and the reference phase (on the contrary to the HT Co_3O_4 diffraction pattern, the (220) line is more intense than the (111) one in nanometric material). Such an inversion has already been observed in similar micrometric materials and was explained by the presence of cobalt vacancies in the structure, mainly in the tetrahedral sites.[22,23] Thus, by means of XRD simulations, Tronel et al. have demonstrated that the (220)/(111) line intensity ratio is strongly connected to the cobalt occupancy in tetrahedral sites of such Co_3O_4 spinel type materials[22] (the former decreases exponentially with the latter).

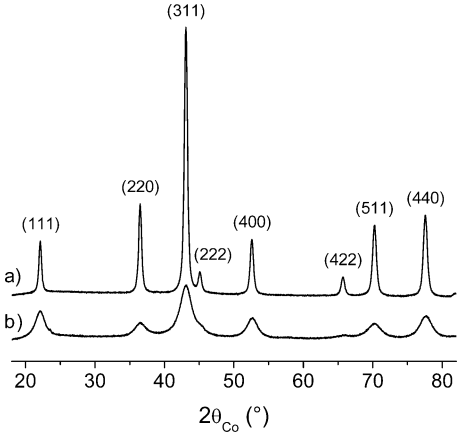

Figure 1. X ray diffraction patterns of (a) reference HT Co_3O_4 and (b) the fresh precipitated material (SP initial), with their indexation in the cubic cell (*Fd*3*m* space group).

In Situ High-Temperature X-ray Diffraction Study. The structural evolution of SP initial was followed by X ray diffraction during heat treatment, as described in the Experimental Section, and the evolution with temperature of the resulting X ray diffraction patterns is displayed in Figure 2. The initial and final diagrams, recorded at room temperature, are respectively denoted as RT i and RT f. Upon the temperature increase, the following modifications can be highlighted. (i) The width of the diffraction lines decreases beyond 200 °C, indicating an increase of the size of the crystalline domains in the material. (ii) The inversion of the (220)/(111) line intensity ratio evidenced in the starting material tends to break up, leading to a ratio similar to that of reference HT Co_3O_4. This suggests a modification of the structure, as well as of the cobalt sites occupancy. (iii) Beyond 400 °C, new diffracted lines emerge and can be assigned to $LiCoO_2$. The appearance of $LiCoO_2$ is particularly highlighted by the splitting of the peak at 22.1° (2θ) in two lines: the (003) line of the $LiCoO_2$ phase and the (111) line of the Co_3O_4 one. Indeed, at room temperature, the (003) line of $LiCoO_2$ is hidden by the (111) line of the Co_3O_4 (RT f), but the two phases can be distinguished at higher temperature (400 to 650 °C) due to different thermal dilatation coefficients. Thus, the (003) line of $LiCoO_2$ is shifting toward low angles with increasing temperature (increase of the cell parameters with thermal dilatation), while the (111) line of the Co_3O_4 is almost not displaced. On the contrary, two new lines appear in the last pattern (RT f) at 43.7 and 53.0° (2θ), which can be respectively assigned to the (101) and (104) lines of $LiCoO_2$. They were hidden by those of Co_3O_4 between 400 and 650 °C, but enable the identification of the $LiCoO_2$ phase in the RT f diffraction pattern.

To clarify this evolution, diffraction data refinements with the Rietveld method were performed on the diffraction patterns recorded during the in situ thermal treatment (see the Experimental Section for details). The comparison of both experimental and calculated diagrams of SP initial at room temperature (RT i) is displayed in Figure 3a and confirms that the material crystallizes in a normal cubic spinel structure. Oxygen ions (32e) form a cubic close packed arrangement, where Co^{2+} ions occupy the tetrahedral sites (8a) and Co^{3+} the octahedral sites (16d). In our model, the oxygen occupancy was fixed to 100% (no significant variation was observed when refining it). Results of the refinement are reported in Table 1. They underline the presence of cobalt vacancies in both tetrahedral and octahedral sites. Indeed, compared to the ideal $Co^{II}[Co^{III}]_2O_4$ phase where 8a and 16d sites are fully occupied, SP initial exhibits a structure where only 67 and 82% of the

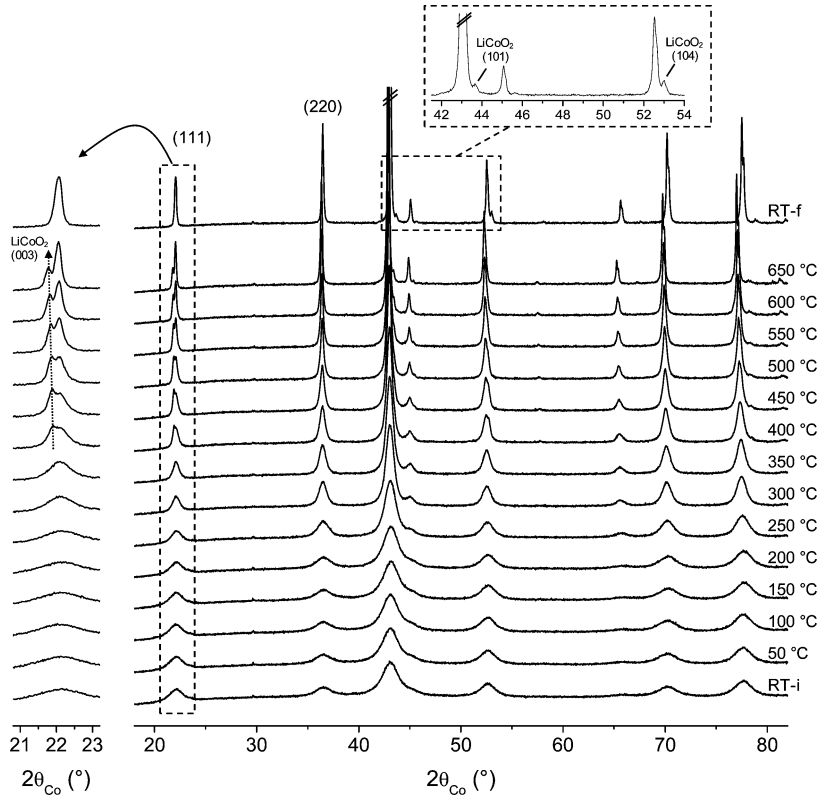

Figure 2. Evolution of the X ray diffraction patterns obtained in situ during thermal treatment of the SP initial material from room temperature (RT i) to 650 °C, with a final cooling down to room temperature (RT f).

latter sites are, respectively, occupied, as proposed to explain the inversion of the (220)/(111) line intensity ratio. Despite the rather good reliability factors obtained for this refinement, the high values of isotropic atomic displacement (between 2 and 3 Å^2) must be pointed out. They could be explained by the nanometric dimensions of the material, which induce strong surface effects,[34] and thus can lead to a distribution of the Co−O bond lengths. One has to keep in mind that in a Ø5 nm spherical particle of an oxide exhibiting a compact lattice, 1/3 of the oxygen atoms belong to the first surface layer.[25] Anyway, occupancy and atomic displacement parameters are strongly correlated and such high isotropic atomic displacement values suggest that the real uncertainty on occupancy values is much higher than the one estimated in the Rietveld refinement. Consequently, in the following of the study, absolute values of occupancy will be considered with caution and we will rather focus on their evolution with temperature.

XRD patterns of SP initial heated at different temperatures were refined in the same way, except for those beyond 400 °C, for which an additional $LiCoO_2$ phase was considered, as discussed above. For example, the experimental and calculated diagrams of the material heated at 650 °C, displayed in Figure 3b, show that three diffractions lines of $LiCoO_2$ can be detected, which enables only a refinement of its cell parameters. Let us note that $LiCoO_2$ exhibits two different structures depending on the synthesis conditions. A HT $LiCoO_2$ layered phase (hexagonal cell, *R*3*m* space group) is usually obtained at high temperature, whereas a LT $LiCoO_2$ spinel type phase (*Fd*3*m* space group) is generally formed below 400 °C.[35] For comparison with the high temperature phase, the XRD pattern of LT $LicoO_2$ can be indexed in a hexagonal cell. The two phases exhibit very similar XRD diagrams, but can be distinguished thanks to the c_{hex}/a_{hex} ratio parameter; it is equal to $2\sqrt{6}$ (4.90) for LT $LiCoO_2$ and close to 4.99 for HT $LiCoO_2$.[36,37] In our case, the c_{hex}/a_{hex} ratio was determined to be 4.99 for the material cooled down to room temperature (RT f). Consequently, based on the value of the c_{hex}/a_{hex} ratio and on the results of Douin et al. in a similar study,[23] we show that the HT $LiCoO_2$ phase may be formed during the XRD in situ analysis. Thus, the HT $LiCoO_2$ structure is described in the hexagonal system (*R*3*m* space group), with oxygen in the 6c position (0, 0, 0.2559), cobalt ions in the 3a sites (0, 0, 0), and lithium ions in the 3b sites (0, 0, 1/2). For this secondary phase, only the lattice parameters (a_{hex} and c_{hex}) and the parameters of the profile function were refined because of its presence in small amounts. In particular, the atomic positions were fixed to values reported in the literature.[23] The results of pattern refinements upon temperature increasing are summar ized in Table 2. Due to the lack of information about the HT $LiCoO_2$ phase (low number of visible peaks), no quantitative analysis could be undertaken. Finally, one can notice that in the case of similar micrometric materials studied by Douin et al.,[23] the HT $LiCoO_2$ phase appears only beyond 500 °C (vs 400 °C in our case). Such a discrepancy can be explained by the nanometric dimensions of our material, that may lower the energy required to achieve the phase separation.

Figure 4a presents the evolution of the cubic cell parameter for the spinel phase obtained during the in situ thermal treatment (full squares). The values obtained for materials annealed ex situ and cooled down to room temperature are also reported (empty squares) and will be commented on in the following. As expected, the cubic lattice parameter globally increases with temperature and decreases upon cooling due to the thermal dilatation of the unit cell. However, two peculiar

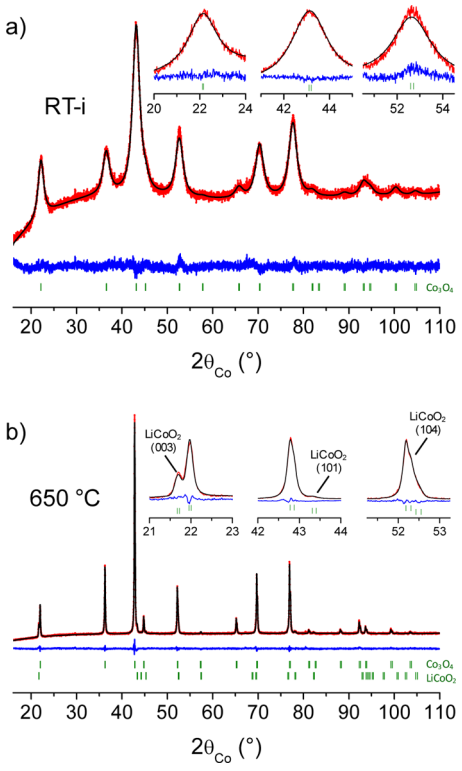

Figure 3. Rietveld refinements of the X ray diffraction patterns of SP initial phase, (a) at room temperature and (b) after a thermal treatment in situ at 650 °C. Each picture shows the experimental (red line) and calculated (black line) X ray powder diffraction patterns, the difference curve between the two profiles (blue line), and the positions of diffraction lines for the Co_3O_4 and $LiCoO_2$ phases (green lines).

phenomena are observed. The lattice parameter (i) decreases with temperature increasing from 25 to around 200 °C, and (ii) does not recover its initial value after the cooling down (it rises from 8.0758 to 8.0805 Å). Those two effects suggest modifications in the structure/composition of the material and will be explained in the chemical composition section. The formation of $LiCoO_2$ has been evidenced beyond 400 °C. Similarly, the temperature dependence of the $LiCoO_2$ cell parameters is plotted in Figure 4b. Both a_{hex} and c_{hex} lattice parameters exhibit a linear variation with temperature, fully explained by thermal dilatation.

The thermal evolution of the cobalt occupancies within the spinel structure is displayed in Figure 5a. As mentioned before, occupancy values are associated with a large uncertainty due to high atomic displacement values. Nevertheless, we can observe that the cobalt occupancy in the 8a tetrahedral sites is subjected to huge modifications with temperature, rising from 67% in the starting material to 93% in the final material (at 650 °C). The evolution in the 16d octahedral sites occupancy is less obvious due to uncertainties and could be assumed to remain quite constant. Consequently, upon increasing temperature, there is a continuous material reconstruction with a decrease of the number of cobalt vacancies, leading to a structure close to that of ideal Co_3O_4. Such a behavior is in agreement with the constant increase of the Co/O ratio displayed in Figure 5b and can be explained by structure reorganization through the departure of oxygen atoms from the spinel structure.

Ex Situ High-Temperature X-ray Diffraction Study. The thermal in situ X ray diffraction performed on SP initial has highlighted enhancement of crystallization upon temperature increasing from room temperature to 650 °C. Moreover, the 100−300 °C range seems to be very interesting since additional phenomena appear (decrease of the cubic cell parameter, increase of Co/O ratio) and since the material is monophasic (HT $LiCoO_2$ appears beyond 400 °C). Thus, the SP initial material has been heat treated ex situ at 100, 150, 200, 250, 300, 400, and 650 °C, to recover easily the material and look further in the mechanisms induced by temperature effect. These ex situ heat treated materials will be denoted as SP 100, SP 150, ..., SP 650 in the following.

X ray patterns of the synthesized phases (not shown here, but presented in Figure S1 in the Supporting Information or in

Table 1. Structural and Profile Parameters, Determined from the Rietveld Refinement of the X ray Diffraction Pattern Recorded for the SP Initial Material

SP-Initial, Co_3O_4 Type Phase, $Fd\bar{3}m$, a_{cub} = 8.076(1) Å						
atom	site	Wyckoff positions			occupancy	B/Å
Co	8a	1/8	1/8	1/8	0.67(2)	2.7(2)
Co	16d	1/2	1/2	1/2	0.82(4)	2.4(1)
O	32e	0.2603(4)	0.2603(4)	0.2603(4)	1	2.7(3)
Conditions of the Run						
	T (K)				300	
	angular range				$10 \leq 2\theta \leq 110°$	
	step scan increment (2θ)				0.0167°	
	zero point				0.05(1)	
	number of fitted parameters				19	
Profile Parameters						
	pseudo-Voigt function				PV = ηL + (1 η)G	
					η = 0.91(2)	
	half-width parameters				$H^2 = U \tan^2\theta + V \tan\theta + W$	
					U = 6.9(8)	
					V = 10(9)	
					W = 0.3(2)	
Conventional Rietveld R-Factors with Bragg Contribution (%)						
R_{wp} = 1.11			R_B = 1.44		χ^2 = 1.44	

Table 2. Structural Parameters of the X ray Diffraction Patterns, Obtained During the In Situ Analysis of the SP Initial Sample

	Co_3O_4 phase, $Fd\bar{3}m$				$LiCoO_2$ phase, $R\bar{3}m$		
			cobalt occupancy				
T/°C	a_{cub}/Å	oxygen position	8a sites	16d sites	Co/O	a_{hex}/Å	c_{hex}/Å
RT-i	8.076(1)	0.2603(4)	0.67(2)	0.82(2)	0.58		
50	8.077(1)	0.2601(4)	0.67(2)	0.82(2)	0.58		
100	8.076(1)	0.2605(4)	0.70(1)	0.85(2)	0.60		
150	8.069(1)	0.2596(4)	0.68(2)	0.83(2)	0.59		
200	8.075(1)	0.2594(4)	0.74(1)	0.85(2)	0.61		
250	8.0870(7)	0.2594(3)	0.82(1)	0.87(1)	0.64		
300	8.0937(4)	0.2603(3)	0.87(1)	0.90(1)	0.67		
350	8.0984(3)	0.2607(2)	0.88(1)	0.91(1)	0.67		
400	8.1041(3)	0.2610(2)	0.90(1)	0.90(1)	0.68	2.828(4)	14.175(3)
450	8.1100(2)	0.2610(2)	0.91(1)	0.90(1)	0.68	2.831(3)	14.191(2)
500	8.1151(2)	0.2614(2)	0.94(1)	0.92(1)	0.70	2.834(4)	14.205(2)
550	8.1204(2)	0.2613(2)	0.93(1)	0.92(1)	0.69	2.836(3)	14.221(2)
600	8.1269(2)	0.2614(3)	0.94(1)	0.92(1)	0.69	2.838(3)	14.244(2)
650	8.1350(1)	0.2616(3)	0.94(1)	0.93(1)	0.70	2.840(3)	14.272(2)
RT-f	8.0805(1)	0.2627(3)	0.93(1)	0.91(1)	0.69	2.816(4)	14.059(4)

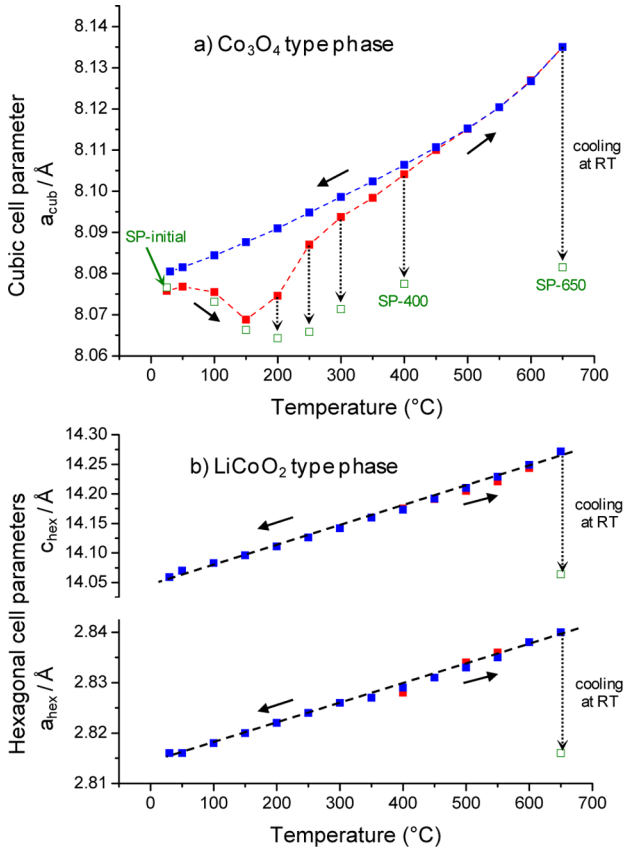

Figure 4. Variations of the cell parameters of (a) the spinel type Co_3O_4 phase and (b) the HT $LiCoO_2$ phase, as deduced from the thermal X ray diffraction in situ analysis (temperature increases up to 650 °C (red square) and then decreases to room temperature (blue square)). The values obtained for materials that were ex situ heat treated (SP initial to SP 650), that is, cooled down to room temperature, are also displayed (green open square). The HT $LiCoO_2$ has been evidenced to appear irreversibly below 400 °C and the superposed points between 400 and 650 °C account for the hexagonal cell parameters upon increasing and decreasing temperatures.

ref 27 have been recorded at room temperature and refined using the Rietveld method. Just as for the thermal in situ analysis, results of the refinements are reported in Table 3. The evolution of the cubic cell parameter with the synthesis temperature is compared in Figure 4a with the in situ results. The same trend, that is, decrease of a_{cub} up to 200 °C, followed by an increase, is observed for both in situ and ex situ analysis. For the latter, no thermal dilatation is involved since the XRD diagrams have been recorded at room temperature, and the evolution evidenced can be only explained by irreversible modifications of the structure and the chemical composition. In particular, the a_{cub} parameter value at the highest temperature is observed to get closer to that of stoichiometric Co_3O_4 (8.088 Å).[38] It is also interesting to note that the spinel phase heated in situ and ex situ at 650 °C leads to the same a_{cub} parameter (8.081 Å) at room temperature. Then, the cobalt occupancy values detailed in Table 3 are in good agreement with those obtained by means of in situ analysis (Table 2). A huge increase can be noticed for cobalt occupancy in tetrahedral sites (from 61% in SP initial to 93% in SP 650), while the occupancy in octahedral sites seems to remain constant at around 85%. Finally, it must be added that HT $LiCoO_2$ is not detected in SP 400 for the reasons detailed previously, that is, the HT $LiCoO_2$ lines are hidden by those of Co_3O_4 due to the broadness of the latter at room temperature.

Particle Size Evolution with Temperature. Figure 6 displays the evolution of average particle sizes (estimated using Sherrer's formula on ex situ XRD patterns) and of specific surface areas as a function of heating temperatures. SP initial shows particles of around 5 nm, whose size remains stable up to 200 °C and then grows. The specific surface area is stable below 200 °C (less than 10% loss) and a huge drop off can be noticed between 200 and 300 °C where it is divided by two. The two evolutions are in good agreement and lead to the same conclusion: the increasing temperature has no effect on particle size up to 200 °C and grain growth can be observed beyond.

2. Chemical Composition. Chemical compositions of SP initial and heat treated samples are summarized in Table 3; data of ideal Co_3O_4 are also reported as reference. Since a pure spinel type "Co_3O_4" phase has been demonstrated to exist only until 300 °C included (an additional HT $LiCoO_2$ phase

dx.doi.org/10.1021/jp3100359 | J. Phys. Chem. C 2013, 117, 9065−9075

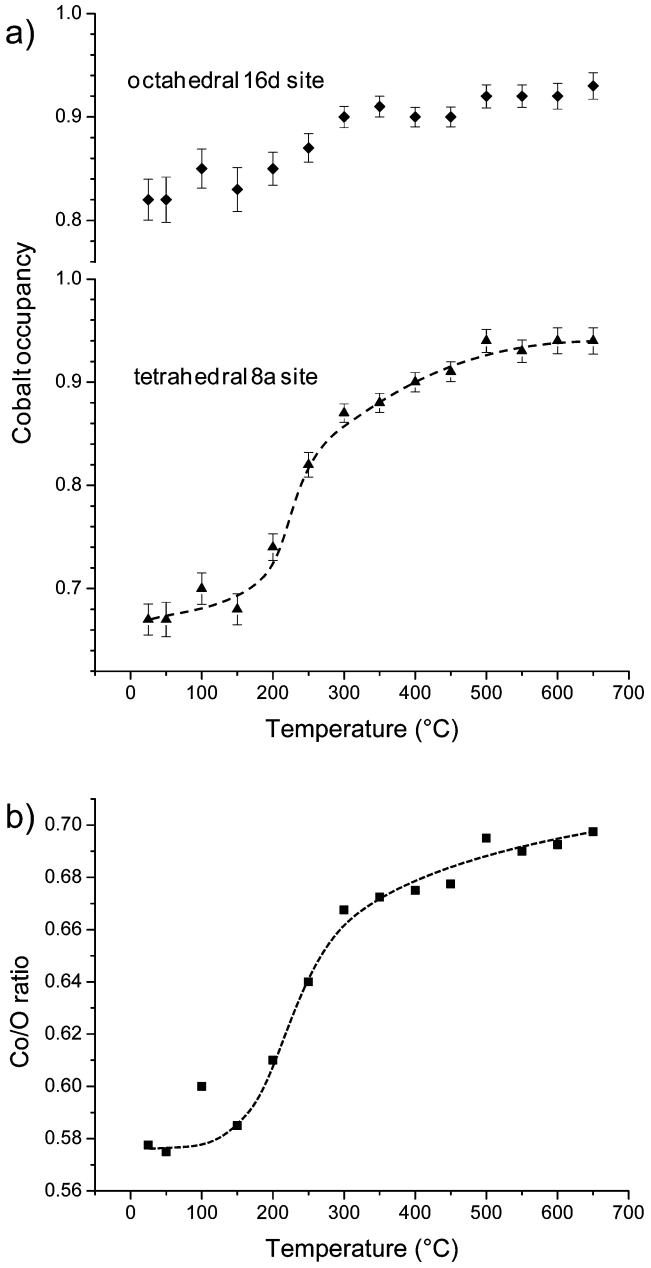

Figure 5. Thermal evolutions of (a) the cobalt occupancy in the 8a tetrahedral sites and in the 16d octahedral sites and (b) the Co/O ratio, as deduced from the Rietveld refinement of the XRD diagrams resulting from the thermal X ray diffraction in situ analysis (from 25 to 650 °C).

emerges beyond 400 °C), the chemical analysis will focus on the study of materials prepared up to 300 °C.

The chemical analysis results show that (i) the amounts of C, N, Na, and K are very low (ratios over Co below 0.01), so they can be neglected. (ii) Significant amounts of hydrogen and lithium were detected in these samples and can be assigned to ions in the spinel structure, since a single phase has been evidenced. The Li/Co ratio remains constant (0.05−0.06) over the considered temperature range. As far as hydrogen is concerned, its amount gradually decreases with the increasing treatment temperature (H/Co = 0.85 for SP initial against 0.23 after heating at 300 °C). Hydrogen can be a priori attributed to protons within the spinel structure and to water adsorbed at the surface of the nanometric particles. The departure of protons is necessarily coupled with that of oxygen from the structure, since TGA analysis under argon coupled with mass spectrometry shows a continuous release of H_2O in the RT to 650 °C range (see Figure S2 in the Supporting Information). This behavior is in accordance with the increase of the Co/O ratio evidenced in the X ray diffraction section. (iii) The Co content in the studied materials is lower than that in ideal Co_3O_4 (73.42 mass%), which is in good agreement with the presence of cobalt vacancies in the spinel structure, but which can also be explained by the presence of additional species in the spinel structure (protons, lithium) or adsorbed water. The Co amount tends anyway to increase with temperature, in agreement with the release of oxygen and the increase of the Co/O ratio. The average oxidation state of cobalt is higher than that expected in an ideal $Co^{II}Co^{III}{}_2O_4$ spinel (2.67), which strongly supports the presence of Co^{4+} ions. It remains quite stable up to 250 °C and then slightly decreases, getting closer to that of ideal spinel.

Formulas were thus established for each ex situ heat treated sample on the basis of chemical analysis results (chemical composition and cobalt oxidation state titration) and crystal refinement data, established in the X ray analysis section (cobalt occupancies in tetrahedral and octahedral sites). For this purpose, Co^{2+} ions are considered to occupy partially the 8a tetrahedral sites, while Co^{3+} and Co^{4+} are supposed to be localized in the 16d octahedral sites. The stoichiometric coefficient of each cobalt ion is evaluated from the occupancies calculated by structural refinement and of the cobalt average oxidation state. Let us remind that the oxygen sites (32e) were supposed to be fully occupied in this model. The overall charge balance is then ensured by all the lithium ions and an adjusted amount of protons. Remaining hydrogen atoms allow finally to determine the amount of adsorbed water molecules. Consid ering these hypotheses, such a typical formula can be written for SP initial:

$$H_{1.34}Li_{0.14}Co^{II}{}_{0.61}[Co^{III}{}_{1.58}Co^{IV}{}_{0.14}]O_4\cdot 0.32H_2O$$

Li ions are supposed to occupy the 8a tetrahedral sites, according to results obtained on micrometric cobalt oxides,[22] even if its location in other sites of the spinel structure (16d, 16c, 8b, 48f) cannot be totally excluded. As shown in the above formula, protons are too numerous to be only located in the cobalt tetrahedral vacancies and might also occupy some other sites of the spinel structure, which are not determined at the present time. Formulas of all heat treated samples have been established in the same way and are reported in Table 3. Their evolution shows, as expected, a decrease in the amounts of structural protons and adsorbed water molecules.

The variation of the Co^{4+}/Co^{3+} ratio in the octahedral sites as a function of the heat treatment temperature can be deduced from the above formulas; it is displayed in Figure 7. The Co^{4+}/Co^{3+} ratio passes through a maximum, reached at 200 °C (0.23), and then goes down. This evolution has to be related to the variation of the cubic cell parameter of the spinel phase (see the X ray diffraction ex situ analysis and Figure 4a) with temperature. Indeed, the general tendency shows an increase of the cell parameter when the synthesis temperature increases from RT up to 650 °C, with a peculiar decreasing phenomenon in the 100−200 °C range. Comparing this evolution with that of the cell parameter, it can be observed that the increase of the Co^{4+}/Co^{3+} ratio is linked to a slight contraction of the lattice.

Partial Discussion. In summary, as reported in the previous sections, upon increasing temperature from room temperature

Table 3. Structural Parameters and Chemical Compositions Determined for Heat Treated Materials, SP Initial to SP 650 (Obtained by Heating Ex Situ the SP Initial Material at Temperatures Ranging from 25 to 650 °C)[a]

	Rietveld analysis				chemical analysis						
			Co occupancy								
synth. T/°C	a_{hex}/Å	oxygen position	8a sites	16 sites	Co wt %	Li wt %	H wt %	Li/Co atomic ratio	H/Co atomic ratio	avg oxidation state of cobalt	formula
initial	8.077(2)	0.2628(6)	0.61(2)	0.86(4)	68.85	0.47	1.00	0.06	0.85	2.80	$H_{1.34}Li_{0.14}Co^{II}_{0.61}[Co^{III}_{1.58}Co^{IV}_{0.14}]O_4{\cdot}0.32H_2O$
100	8.073(2)	0.2612(7)	0.66(3)	0.84(4)	67.13	0.42	0.97	0.05	0.84	2.83	$H_{1.25}Li_{0.13}Co^{II}_{0.66}[Co^{III}_{1.42}Co^{IV}_{0.26}]O_4{\cdot}0.36H_2O$
150	8.067(3)	0.2604(8)	0.68(3)	0.83(5)	66.97	0.42	0.93	0.05	0.81	2.83	$H_{1.28}Li_{0.12}Co^{II}_{0.68}[Co^{III}_{1.37}Co^{IV}_{0.28}]O_4{\cdot}0.31H_2O$
200	8.064(2)	0.2588(6)	0.69(2)	0.81(3)	68.14	0.42	0.85	0.05	0.73	2.83	$H_{1.37}Li_{0.12}Co^{II}_{0.69}[Co^{III}_{1.31}Co^{IV}_{0.30}]O_4{\cdot}0.16H_2O$
250	8.066(2)	0.2596(5)	0.75(2)	0.84(3)	68.13	0.42	0.57	0.05	0.49	2.81	$H_{1.04}Li_{0.13}Co^{II}_{0.75}[Co^{III}_{1.39}Co^{IV}_{0.29}]O_4{\cdot}0.07H_2O$
300	8.071(2)	0.2597(6)	0.83(3)	0.86(3)	73.40	0.45	0.29	0.05	0.23	2.77	$H_{0.80}Li_{0.13}Co^{II}_{0.83}[Co^{III}_{1.48}Co^{IV}_{0.24}]O_4{\cdot}0.00H_2O$
400	8.0775(5)	0.2622(3)	0.84(2)	0.90(2)	73.42	0.45	0.08	0.05	0.06	2.75	"$Li_xCo_{3-\delta}O_4$ + $LiCoO_2$"
650	8.0815(1)	0.2620(2)	0.93(1)	0.92(2)	73.66	0.46	0.02	0.05	0.02	2.75	"$Li_xCo_{3-\delta}O_4$ + $LiCoO_2$"
ideal Co_3O_4		0.2631	1	1	73.42					2.67	$Co^{II}[Co^{III}_2]O_4$

[a]Corresponding formulae were established on the basis of cobalt occupancies determined by Rietveld refinement and chemical analysis. Values for ideal Co_3O_4 are also reported.

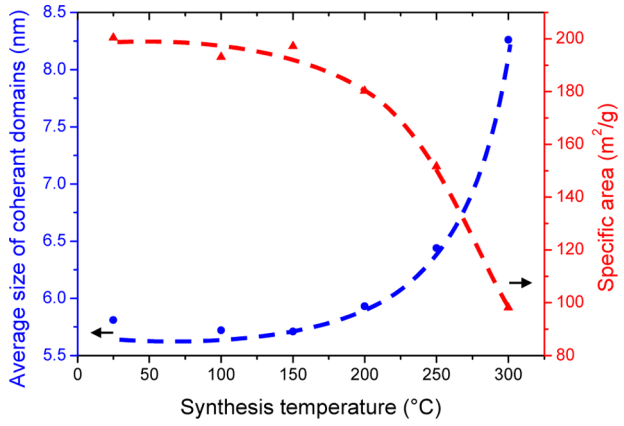

Figure 6. Evolution of average sizes of coherent domains (deduced from Scherrer formula; blue circle) and of specific surface areas (BET measurements; red triangle) for spinel type materials, heat treated at temperatures ranging from 25 to 300 °C.

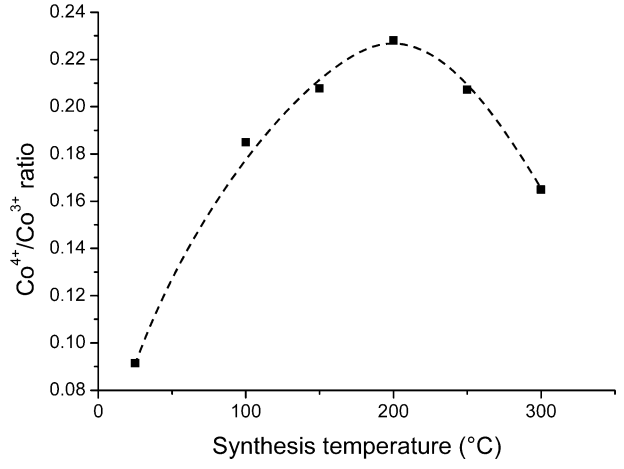

Figure 7. Variation of the Co^{4+}/Co^{3+} ratio (deduced from Rietveld refinement and chemical analysis) in spinel type materials, heat treated at temperatures ranging from 25 to 650 °C.

to 650 °C, the following structural and composition modifications have been evidenced: (i) a continuous release of hydrogen, (ii) an increase of the amount of cobalt in the tetrahedral sites while the octahedral occupancy remains stable, (iii) a stabilization of the average oxidation state of cobalt below 200 °C, followed by a decrease, and (iv) an increase of the Co^{4+}/Co^{3+} ratio up to 200 °C, which then decreases. All these effects can be explained as already reported for similar micrometric materials.[23] When temperature increases, the departure of protons from the lattice entails a reorganization within the spinel structure, with a filling of the tetrahedral sites, where only Co^{2+} ions are stable from crystal field consid erations, and an increase of the Co/O ratio. The departure of protons is finally balanced by an increase of the Co^{4+}/Co^{3+} ratio in the octahedral network.

3. Electronic Properties. Electronic properties of the ex situ heat treated materials were investigated under air in the 25 to 300 °C range, which corresponds to the spinel single phase domain. Figure 8 compares the temperature dependence of electronic conductivity for HT Co_3O_4, SP initial, SP 200, and SP 300. The curves corresponding to the materials synthesized at 100, 150, and 250 °C are not reported for more clarity. Nevertheless, Figure 9 presents the conductivity values for all the synthesis temperatures. As shown by the arrows in Figure 8, the measurements were performed by increasing temperature from RT to 400 °C, and then decreasing down to RT, giving rise to a singular curve shape, involving two different domains: a strong and irreversible conductivity increase up to 400 °C, followed by a quasi linear conductivity decrease when temper ature goes down to 25 °C. The curve parts that correspond to decreasing temperatures are completely reversible and fully reproducible when increasing−decreasing temperature cycles are performed afterward. They characterize the electronic behavior of the materials after heating at 400 °C, whatever the initial synthesis temperature. These behaviors correspond to a hopping type mechanism, with activation energies in the 0.01−0.04 eV range, as expected for semiconductor materials. On the contrary, the curve parts that correspond to increasing temperatures are irreversible and are likely to result from three different contributions, occurring at different scales, and all leading to an increase of conductivity with temperature. (i) The first effect results from the fact that, at the microscopic scale, increasing temperature induces a sintering of the pellet, as suggested by the increase of the size of coherent domains,

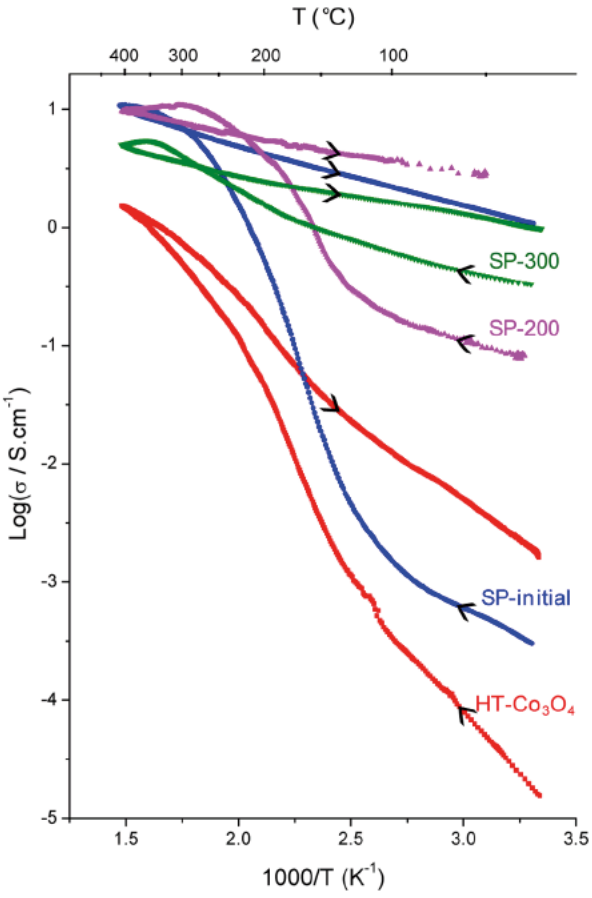

Figure 8. Variation of the logarithm of electrical conductivity versus reciprocal temperature for reference HT Co_3O_4, SP initial, SP 200, and SP 300 materials. Temperature was increased up to 400 °C and then cooled down to room temperature.

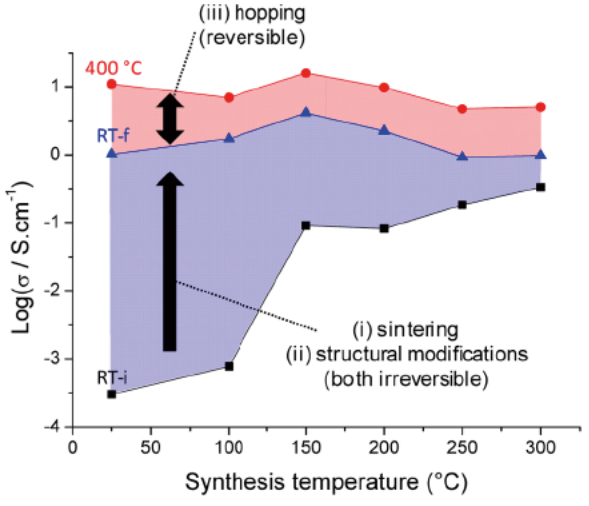

Figure 9. Values of the logarithm of electrical conductivity at room temperature before the electronic measurement (black square), at 400 °C (red circle), and at RT after the electronic measurement (blue triangle), that is, an increase of temperature up to 400 °C, followed by a decrease, for spinel materials heat treated at temperatures ranging from 25 to 300 °C.

deduced from X ray diffraction data, and shown in Figure 6. The grain boundaries are thus reduced and the particle size increases, resulting in an irreversible increase of conductivity. (ii) The second contribution is due to the structural and composition modifications induced by heating. (iii) The third contribution to conductivity enhancement with temperature is linked to the hopping effect, as mentioned just above for the second curve parts.

At room temperature, conductivity of reference HT Co_3O_4 is quite low ($\sigma_{RT} = 1.6 \times 10^{-5}$ S·cm^{-1}), in accordance with its well known insulating behavior, whereas that of heat treated spinel phases is much higher (more than 2 orders of magnitude). Such a high conductivity was already observed in our group for similar micrometric spinel cobalt phases, prepared by electrooxidation in an alkaline lithiated electrolyte.[22] It was proven to be linked to the presence of hydrogen, lithium, and tetravalent cobalt in octahedral sites. Indeed, the presence of a mixed valency Co^{4+}/Co^{3+} (t_{2g}^5/t_{2g}^6) in the octahedral network induces holes in the t_{2g} band and entails an electronic delocalization through the overlapping of the cobalt t_{2g} orbitals, resulting therefore in good electronic conductivity. Nevertheless, the moderate amount of holes in the t_{2g} band, as well as the presence of defects (cobalt vacancies, hydrogen, lithium), which tend to locally trap the holes, prevents from a real metallic behavior. A hopping between the local metallic domains was rather envisaged, as supported by Li NMR data and thermoelectric power measurements.[22] The conductivity value at room temperature for the nanometric spinel phases reaches a maximum (around 10^{-1} S·cm^{-1}) as soon as the synthesis temperature is around 150−200 °C, as shown in Figure 9. This behavior must be linked to the variation of the Co^{4+}/Co^{3+} ratio (Figure 7), which reaches a maximum just at 200 °C. The conductivity is indeed all the more better as the Co^{4+}/Co^{3+} ratio in the octahedral network is higher, because the presence of Co^{4+} ions promotes electronic delocalization.

Comparison of the conductivity curves of SP initial, SP 200, and SP 300 in Figure 9 shows that the conductivity values at RT at the very end of the measurements, that is, after increasing and then decreasing temperature, are very close to each other (at around 5 S·cm^{-1}). This behavior was expected because, at this stage, all the materials have been subjected to the same treatment at 400 °C (during the first part of conductivity measurement). It should be added that the conductivity enhancement is much larger in the case of SP initial (about 4 orders of magnitude) than for SP 200 and SP 300 (about 1 order of magnitude), because the contribution of the structural modifications (effect (ii), as previously mentioned) to the conductivity increase is very large for SP initial, whereas as prepared SP 200 and SP 400 should have already reached their maximum conductivity (see Figure 9). The conductivity enhancement observed in the latter cases is essentially due the grain coalescence effect in the pellet. As shown in Figure 8, the conductivity increase is also moderate for HT Co_3O_4 because it undergoes no structural modification, just the sintering effect. Considering the activation energies of the second curve domains (decreasing temperature), similar values should be expected for all the materials, because they were all heated up to 400 °C during the first step of conductivity measurement. As a matter of fact, discrepancies are observed, as shown by the curve slopes in Figure 8 (0.04 eV for SP initial, 0.03 eV for SP 100 and 0.01−0.03 eV for materials synthesized at temperatures higher than 150 °C). They probably result from a kinetic effect, the composition of the final materials being strongly dependent on the total thermal treatment duration (initial synthesis + conductivity measurement).

CONCLUSION

This work has investigated the temperature dependence of a nanometric spinel type conductive $H_xLi_yCo_{3-\delta}O_4 \cdot zH_2O$ phase prepared by low temperature precipitation. Upon increasing temperature, modifications occur simultaneously in the chemical composition and in the structure, leading to an increase of the Co^{4+}/Co^{3+} ratio in the octahedral network, with a maximum value for a treatment temperature around 200 °C. The electronic conductivity, which results from a delocalization effect in the octahedral network, linked to the presence of Co^{4+} ions, tends therefore to follow the Co^{4+}/Co^{3+} ratio. The materials that are heat treated at temperatures between 150 and 300 °C exhibit the highest conductivity at room temperature, around 10^{-1} S·cm^{-1}, against about 10^{-4} S·cm^{-1}, for the pristine spinel phase.

As we recently reported,[26] the electrochemical behavior of this pristine material as positive electrode of supercapacitor is quite interesting, leading to capacity of 320 F/g in 8 M KOH, with a very small amount of carbon black added (5%). The similar heat treated materials, which exhibit a RT conductivity that is 3 orders of magnitude higher, appear therefore as promising candidates for the same application. Nevertheless, the design of supercapacitor materials requires finding the best compromise between electronic conductivity, which is at the top for the material annealed at 250 °C, and specific surface area, which shows highest BET areas up to 200 °C. The material that is heat treated at 200 °C appears therefore to be a good candidate (σ_{RT} = 0.083 S·cm^{-1}, 180 m^2/g) as electrode material and will be investigated in hybrid supercapacitor systems in future studies.

ASSOCIATED CONTENT

Supporting Information

Two additional figures are given in Supporting Information. The first one (Figure S1) shows the X ray diffraction patterns of SP initial and the heat treated materials (SP 100 to SP 650). The second one (Figure S2) is the TGA measurement (coupled with mass spectroscopy) of the SP initial compound which evidence a continuous proton departure in the 25−650 °C range. This material is available free of charge via the Internet at http://pubs.acs.org.

AUTHOR INFORMATION

Corresponding Author

*Phone: +33 (0) 5 40 00 27 25. Fax: +33 (0) 40 00 27 61. E mail: guerlou@icmcb bordeaux.cnrs.fr.

Notes

The authors declare no competing financial interest.

ACKNOWLEDGMENTS

The authors would like to thank C. Denage and P. Dagault for technical assistance, and the French National Agency for Research (ANR, Stock E 2008 program, SupECCO project) for financial support.

REFERENCES

(1) Grillo, F.; Natile, M. M.; Glisenti, A. Low Temperature Oxidation of Carbon Monoxide: the Influence of Water and Oxygen on the Reactivity of a Co_3O_4 Powder Surface. *Appl. Catal., B* **2004**, *48*, 267−274.

(2) Wang, Y. Z.; Zhao, Y. X.; Gao, C. G.; Liu, D. S. Preparation and Catalytic Performance of Co_3O_4 Catalysts for Low Temperature CO Oxidation. *Catal. Lett.* **2007**, *116*, 136−142.

(3) Irfan, M. F.; Goo, J. H.; Kim, S. D. Co_3O_4 Based Catalysts for NO Oxidation and NO_x Reduction in Fast SCR Process. *Appl. Catal., B* **2008**, *78*, 267−274.

(4) Li, W. Y.; Xu, L. N.; Chen, J. Co_3O_4 Nanomaterials in Lithium Ion Batteries and Gas Sensors. *Adv. Funct. Mater.* **2005**, *15*, 851−857.

(5) Cao, A. M.; Hu, J. S.; Liang, H. P.; Song, W. G.; Wan, L. J.; He, X. L.; Gao, X. G.; Xia, S. H. Hierarchically Structured Cobalt Oxide (Co_3O_4): the Morphology Control and Its Potential in Sensors. *J. Phys. Chem. B* **2006**, *110*, 15858−15863.

(6) Makhlouf, S. A. Magnetic Properties of Co_3O_4 Nanoparticles. *J. Magn. Magn. Mater.* **2002**, *246*, 184−190.

(7) Ichiyanagi, Y.; Kimishima, Y.; Yamada, S. Magnetic Study on Co_3O_4 Nanoparticles. *J. Magn. Magn. Mater.* **2004**, *272−276*, E1245−E1246.

(8) Thackeray, M.; Baker, S.; Adendorff, K.; Goodenough, J. Lithium Insertion into Co_3O_4: a Preliminary Investigation. *Solid State Ionics* **1985**, *17*, 175−181.

(9) Larcher, D.; Sudant, G.; Leriche, J. B.; Chabre, Y.; Tarascon, J. M. The Electrochemical Reduction of Co_3O_4 in a Lithium Cell. *J. Electrochem. Soc.* **2002**, *149*, A234−A241.

(10) Lin, C.; Ritter, J. A.; Popov, B. N. Characterization of Sol Gel Derived Cobalt Oxide Xerogels as Electrochemical Capacitors. *J. Electrochem. Soc.* **1998**, *145*, 4097−4103.

(11) Xiong, S.; Yuan, C.; Zhang, X.; Xi, B.; Qian, Y. Controllable Synthesis of Mesoporous Co_3O_4 Nanostructures with Tunable Morphology for Application in Supercapacitors. *Chem.—Eur. J.* **2009**, *15*, 5320−5326.

(12) An, K. H.; Kim, W. S.; Park, Y. S.; Choi, Y. C.; Lee, S. M.; Chung, D. C.; Bae, D. J.; Lim, S. C.; Lee, Y. H. Supercapacitors Using Single Walled Carbon Nanotube Electrodes. *Adv. Mater.* **2001**, *13*, 497−500.

(13) Appandairajan, N. K.; Viswanathan, B.; Gopalakrishnan, J. Lithium Substituted Cobalt Oxide Spinels $Li_xM_{1-x}Co_2O_4$ (M = Co^{2+}, Zn^{2+}; $0 \le x \le 0.4$). *J. Solid State Chem.* **1981**, *40*, 117−121.

(14) Holgersson, S.; Karlsson, A. Über einige Neue Kobaltite vom Spineltypus. *Z. Anorg. Allg. Chem.* **1929**, *183*, 384−394.

(15) Pyke, D.; K. Mallick, K.; Reynolds, R.; Bhattacharya, K. A. Surface and Bulk Phases in Substituted Cobalt Oxide Spinels. *J. Mater. Chem.* **1998**, *8*, 1095−1098.

(16) Tareen, J.; Malecki, A.; Doumerc, J.; Launay, J.; Dordor, P.; Pouchard, M.; Hagenmuller, P. Hierarchically Porous Ni Co Oxide for High Reversibility Asymmetric Full Cell Supercapacitors. *Mater. Res. Bull.* **1984**, *19*, 989−997.

(17) Asano, K.; Ohnishi, C.; Iwamoto, S.; Shioya, Y.; Inoue, M. Potassium Doped Co_3O_4 Catalyst for Direct Decomposition of N_2O. *Appl. Catal., B* **2008**, *78*, 242−249.

(18) Rasiyah, P.; Tseung, A. C. C. A Mechanistic Study of Oxygen Evolution on Li Doped Co_3O_4. *J. Electrochem. Soc.* **1983**, *130*, 365−368.

(19) Zhecheva, E.; Stoyanova, R.; Angelov, S. Doping of Co_3O_4 with Lithium by a Solid State Reaction in Air. I. Oxidation Degree and Coordination of Cations. *Mater. Chem. Phys.* **1990**, *25*, 351−360.

(20) Antolini, E. Formation of Lithium Cobalt Spinel Oxide ($Li_xCo_{3-x}O_4$) by Solid State Reaction of a Li_2CO_3−Co_3O_4 Powder Mixture. *Mater. Res. Bull.* **1997**, *32*, 9−14.

(21) Zhecheva, E.; Stoyanova, R. Low Temperature Preparation of a Lithium Cobalt Spinel ($Li_{0.35}Co_{2.65}O_4$) by Thermal Decomposition of CoOOH in a $LiNO_3$ Melt. *Mater. Res. Bull.* **1991**, *26*, 1315−1322.

(22) Tronel, F.; Guerlou Demourgues, L.; Ménétrier, M.; Croguennec, L.; Goubault, L.; Bernard, P.; Delmas, C. New Spinel Cobalt Oxides, Potential Conductive Additives for the Positive Electrode of Ni MH Batteries. *Chem. Mater.* **2006**, *18*, 5840−5851.

(23) Douin, M.; Guerlou Demourgues, L.; Ménétrier, M.; Bekaert, E.; Goubault, L.; Bernard, P.; Delmas, C. Effect of Thermal Treatment on the Electronic Conductivity Properties of Cobalt Spinel Phases

Synthesized by Electro Oxidation in Ternary Alkaline Electrolyte (KOH, LiOH, NaOH). *Chem. Mater.* **2008**, *20*, 6880−6888.
(24) Douin, M.; Guerlou Demourgues, L.; Ménétrier, M.; Bekaert, E.; Goubault, L.; Bernard, P.; Delmas, C. Improvement by Heating of the Electronic Conductivity of Cobalt Spinel Phases, Electrochemically Synthesized in Various Electrolytes. *J. Solid State Chem.* **2009**, *182*, 1273−1280.
(25) Shaju, K. M.; Guerlou Demourgues, L.; Godillot, G.; Weill, F.; Delmas, C. Strategies for Synthesizing Conductive Spinel Cobalt Oxide Nanoparticles for Energy Storage Applications. *J. Electrochem. Soc.* **2012**, *159*, A1934−A1940.
(26) Godillot, G.; Guerlou Demourgues, L.; Taberna, P. L.; Simon, P.; Delmas, C. Original Conductive Nano Co_3O_4 Investigated as Electrode Material for Hybrid Supercapacitors. *Electrochem. Solid State Lett.* **2011**, *14*, A139−A142.
(27) Godillot, G.; Huo, H.; Ménétrier, M.; Bourgeois, L.; Guerlou Demourgues, L.; Delmas, C. Promising Nanometric Spinel Cobalt Oxides for Electrochemical Energy Storage: Investigation of Li and H Environments by NMR. *J. Phys. Chem. C* **2012**, *116*, 26598−26607.
(28) Rietveld, H. M. A Profile Refinement Method for Nuclear and Magnetic Structures. *J. Appl. Crystallogr.* **1969**, *2*, 65−71.
(29) Rodriguez Carvajal, J. FULLPROF: a Program for Rietveld Refinement and Pattern Matching Analysis. *Abstracts of the Satellite Meeting on Powder Diffraction of the XV IUCr Congress, Toulouse, France*, IUCr, Chester (U.K.), 1990, p 127.
(30) Sing, K. S. W.; Everett, D. H.; Haul, R. A. W.; Moscou, L.; Pierotti, R. A.; Rouquerol, J.; Siemieniewska, T. Reporting Physisorption Data for Gas/Solid Systems with Special Reference to the Determination of Surface Area and Porosity. *Pure Appl. Chem.* **1985**, *57*, 603−619.
(31) Emmett, P. H.; Brunauer, S. The Use of Low Temperature Van der Waals Adsorption Isotherms in Determining the Surface Area of Iron Synthetic Ammonia Catalysts. *J. Am. Chem. Soc.* **1937**, *59*, 1553−1564.
(32) Brunauer, S.; Emmett, P. H.; Teller, E. Adsorption of Gases in Multimolecular Layers. *J. Am. Chem. Soc.* **1938**, *60*, 309−319.
(33) Laplume, J. Bases Théoriques de la Mesure de Résistivité et de la Constante de Hall par la Méthode des Quatre Pointes. *L'Onde Electrique* **1955**, *335*, 113−125.
(34) Weirich, T.; Winterer, M.; Seifried, S.; Hahn, H.; Fuess, H. Rietveld Analysis of Electron Powder Diffraction Data from Nano crystalline Anatase, TiO_2. *Ultramicroscopy* **2000**, *81*, 263−270.
(35) Antolini, E. $LiCoO_2$: Formation, Structure, Lithium and Oxygen Nonstoichiometry, Electrochemical Behaviour and Transport Proper ties. *Solid State Ionics* **2004**, *170*, 159−171.
(36) Gummow, R.; Thackeray, M.; David, W.; Hull, S. Structure and Electrochemistry of Lithium Cobalt Oxide Synthesized at 400 °C. *Mater. Res. Bull.* **1992**, *27*, 327−337.
(37) Shao Horn, Y.; Hackney, S.; Johnson, C.; Kahaian, A.; Thackeray, M. Structural Features of Low Temperature $LiCoO_2$ and Acid Delithiated Products. *J. Solid State Chem.* **1998**, *140*, 116−127.
(38) Roth, W. L. The Magnetic Structure of Co_3O_4. *J. Phys. Chem. Solids* **1964**, *25*, 1−10.